On redundancy resolution and energy consumption of kinematically redundant planar parallel manipulators

Andrés Gómez Ruiz, João Cavalcanti Santos, Jan Croes, Wim Desmet, Maíra Martins da Silva

On redundancy resolution and energy consumption of kinematically redundant planar parallel manipulators

Andrés Gómez Ruiz†, João Cavalcanti Santos†, Jan Croes‡§, Wim Desmet‡§ and Maíra Martins da Silva†*

†Department of Mechanical Engineering, São Carlos School of Engineering, University of São Paulo, Av. Trabalhador São-Carlense, 400, 13566-590 São Carlos-SP, Brazil.
E-mails: andresgomezruiz@usp.br, joao.cv.santos@gmail.com
‡Production Engineering, Machine Design and Automation (PMA) Section, Katholieke Universiteit Leuven, Celestijnenlaan 300, 3001 Leuven, Belgium. E-mails: jan.croes@kuleuven.br, wim.desmet@kuleuven.be
§Flanders Make, Oude Diestersebaan 133, 3920 Lommel, Belgium

SUMMARY

Novel kinematic architectures can be alternatives for designing energy efficient robotic systems. In this work, the impact of kinematic redundancies in the energy consumption of a planar PKM, the 3PRRR manipulator, is experimentally verified. Because of the presence of the kinematic redundancies, the inverse kinematic problem presents infinity solutions. In this way, a redundancy resolution scheme based on the Model Predictive Control technique is proposed and exploited. It can be concluded that the energy consumption of the non-redundant parallel manipulator 3RRR for executing predefined tasks can be considerably reduced by the inclusion of kinematic redundancies.

KEYWORDS: Parallel kinematic manipulators; Kinematic redundancy; Energy consumption; Model Predictive control; Redundancy resolution.

1. Introduction

Due to their kinematic architecture, parallel kinematic manipulators (PKMs) are composed of lighter moving parts. As a result, this architecture is a promising alternative for designing not only robotic manipulators with improved dynamic performance[1] but also energy efficient robotic systems.[2] A comparison between serial and parallel kinematic architectures for a three degrees-of-freedom (DOFs) spatial manipulator has been done by ref. [2]. It could be concluded that for similar workspace and actuators, the energy consumption of the PKM was up to 26% smaller than the consumption of the serial manipulator. The main reason for this reduction is the fact that the mass of the moving parts of the parallel manipulator is indeed significantly smaller.

Despite this interesting attribute, PKMs suffer from the presence of singularities in their workspace.[3] Due to the presence of these singularities, the workspace of PKMs is rather limited imposing an important drawback. To overcome this, some researchers have explored the use of redundancy for reducing the singularities' regions.[4–8] Besides the enlargement of the workspace due to the reduction of the singularities' regions, the addition of redundancy might also provide higher accuracy,[9] better motion/force transmissibility,[10] improved dynamic performance,[11,12] among others. A recent review of redundant PKMs has discussed the impact of the use of redundancies on the workspace enlargement, singularity elimination/avoidance, and improved joint-torque distribution.[13]
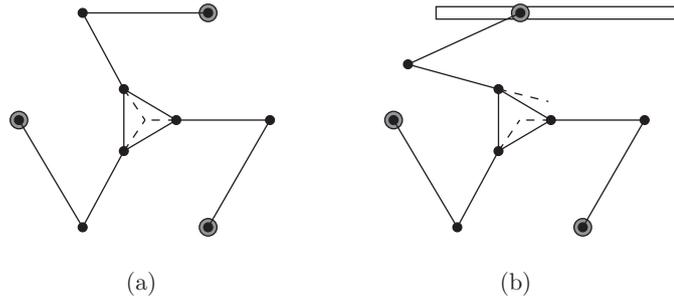
* Corresponding author. E-mail: mairams@sc.usp.br

Fig. 1. Comparison between the end-effector's pose of (a) the non-redundant manipulator 3RRR and (b) the kinematically redundant manipulator 2RRR+PRRR.

According to the manipulator's mobility, two main kinds of redundancy can be used: the kinematic and the actuation redundancy.[13] The number of actuators is higher than the DOFs of the manipulator's end-effector for both strategies. The terminology of redundant parallel manipulators is discussed in-depth in ref. [14]. On the one hand, the actuation redundancy can be implemented by the actuation of passive joints or by the inclusion of active kinematic chains.[12–14] In this case, the inverse kinematic problem presents a unique solution. On the other hand, the kinematic redundancy can be implemented by the introduction of extra active joints in a kinematic chain.[12–14] In this case, the inverse kinematic problem presents infinite solutions. In other words, kinematically redundant PKMs present infinite possible kinematic configurations for a single pose of the manipulator's end-effector. Due to this characteristic, redundancy resolution schemes can be exploited allowing the manipulator to avoid singularities.[15,16]

For sake of illustration, Fig. 1 shows the planar 3RRR PKM and the kinematically redundant planar 2RRR+PRRR PKM. The same end-effector's pose for both manipulators is depicted. These manipulators present three kinematic chains composed of active prismatic joints (P), illustrated by the rectangular form, active revolute joints (R), illustrated by the grey circles, and passive revolute joints (R), illustrated by the black circles. These kinematic chains are connected to the manipulator's end-effector, illustrated by a triangular form, which presents 3-DOFs. In this figure, the end-effector of the 3RRR is at a singular position since the intersection points of the lines of action of each kinematic chain are at the same location. Due to the introduction of an active prismatic joint, the end-effector of the 2RRR+PRRR is not at a singular position demonstrating the capability of kinematically redundant manipulators to avoid singularities.

Redundancy resolution schemes aid the designer to select a proper kinematic configuration, e.g., a reasonable distance away from a singularity, among the infinite possibilities (as illustrated in Fig. 1). These schemes can be posed as optimization problems that can be solved locally or globally.[15] Generally, local approaches formulate the problem by imposing kinematic constraints. These constraints/relations can be formulated using gradient projection methods, Jacobian-based strategies, among others.[16] Whilst local approaches exploit local indexes, global approaches consider the global manipulator's performance. In this way, most global approaches seek to find the optimal inputs for the active joints for a given trajectory of the end-effector (tracking problems). This can be accomplished by defining a cost function.[15] Some authors exploited cost functions related to kinematic[17,18] and dynamic[4,12] performance indexes. In this manuscript, a Model Predictive Path-Following Control scheme is proposed and exploited as a global redundancy resolution scheme. This proposal is based on the Model Prediction Control (MPC) technique that have been employed for tracking problems of industrial serial robots,[19] for vibration reduction of a tower crane prototype,[20] for trajectory planning of autonomous vehicles,[21] among others. Regarding redundant PKMs, MPC techniques have been exploited for deriving control strategies for redundantly actuated PKM.[22–25] For instance, the technique has been used for deriving a force/position control scheme for a 5-DOF redundant actuation parallel manipulator[23] and for deriving an augmented PD control for a planar 2-DOF redundantly actuated PKM.[24] In fact, one of the main contributions of this manuscript is the proposal of a redundancy resolution scheme for kinematically redundant manipulators using MPC technique.
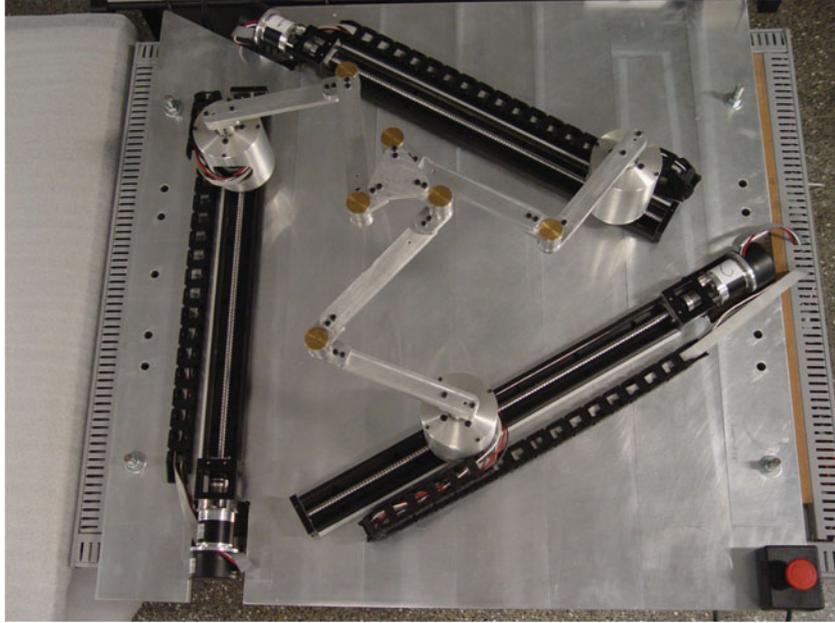
Fig. 2. The 3PRRR prototype.

Recently,[25] claimed that the presence of redundant actuators can yield energy savings. The authors evaluated the energy loss of a 2-DOF kinematically redundant manipulator using numerical results depicted on the workspace. Moreover, numerical studies of the impact of several levels of kinematic redundancies on the required torque[12] and on the energy consumption[26] to perform a predefined trajectory using global redundancy resolution schemes (tracking trajectory) demonstrate that kinematic redundancy can be beneficial to the design of energy efficient manipulators. These conclusions indicate that further investigations should be performed considering torque requirements and energy consumption of kinematically redundant PKMs. In fact, no experimental results are available in the literature.

In this manuscript, the energy consumption of planar kinematically redundant PKMs is experimentally verified and compared using a MPC-based redundancy resolution scheme. The objective of this comparison is to evaluate experimentally whether a planar PKM can benefit from the use of one, two, or three levels of kinematic redundancy in terms of energy consumption. To that end, different kinematic architectures, non-redundant and redundant ones, are compared. The 3PRRR prototype, depicted in Fig. 2, presents three kinematic chains composed of one active prismatic joint (P), one active revolute joint (R), and two passive revolute joints (RR). This versatile setup can be exploited to study the non-redundant manipulator 3RRR by locking the prismatic joints and to study the redundant manipulators PRRR+2RRR, 2PRRR+RRR, and 3PRRR by actuating the prismatic joints. By actuating or locking the prismatic joints eight configurations can be experimentally investigated as illustrated in Fig. 3. In this figure, the revolute joints are illustrated as circles and the prismatic joints as rectangles. The passive prismatic joints are represented by black rectangular forms, the active prismatic joints by white rectangular forms and the active revolute joints are represented by grey circles. Considering these representations, the configuration R1 represents the non-redundant 3RRR PKM ($M = 0$), the configurations R2–R4 represent the possible redundant PRRR+2RRR PKMs ($M = 1$), the configurations R5-R7 represent the possible redundant 2PRRR+RRR PKMs ($M = 2$), and the configuration R8 represents the 3PRRR PKM ($M = 3$), where M is the number of redundant actuators. It is important to highlight that since the energy consumption is task-dependent, these configurations represents different manipulators.

The rest of the manuscript is organized as it follows. Section 2 describes the inverse kinematic model of the non-redundant and redundant manipulators. Section 3 details the redundancy resolution scheme based on the MPC technique. The experimental campaign is described in Section 4, whilst the experimental results are presented in Section 5. Conclusions are drawn in Section 6.
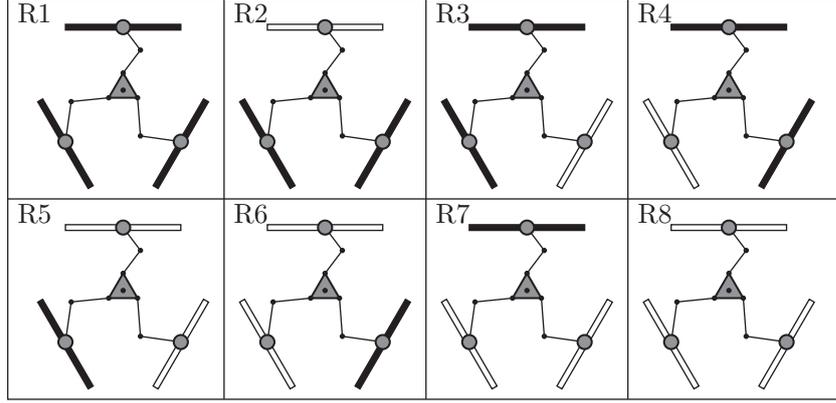
Fig. 3. R1 ($M = 0$): the 3RRR manipulator, R2–R4 ($M = 1$): the PRRR+2RRR manipulators, R5–R7 ($M = 2$): the 2PRRR+RRR manipulators and R8 ($M = 3$): the 3PRRR.
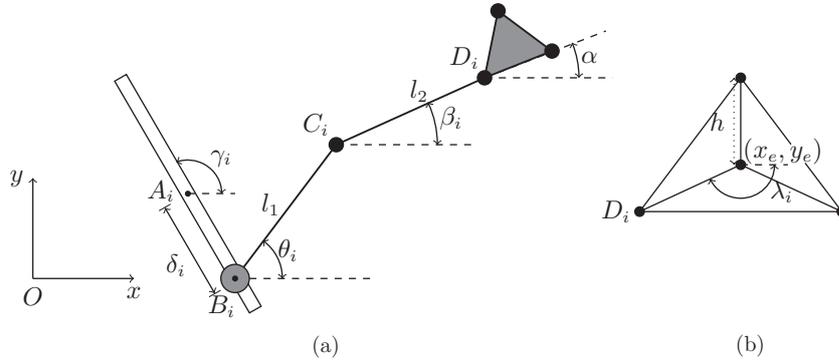

(a)   (b)

Fig. 4. A single kinematic chain (a). End-effector (b).

2. The 3PRRR PKM's Inverse Kinematic Model

The inverse kinematic model provides the mathematical expressions that relate the end-effector's pose, $\mathbf{X} = [x_e \quad y_e \quad \alpha]$, with the joint coordinates, $\mathbf{\Theta} = [\theta_1 \quad \theta_2 \quad \theta_3 \quad \delta_1 \quad \delta_2 \quad \delta_3]$. Those equations are essential for planning the motion of robotic manipulators. Due to the 3PRRR architecture, the inverse kinematic model can be formulated using a single kinematic chain represented by the sub-index i. For this manipulator, the sub-index i can be 1, 2, or 3.

Figure 4 illustrates the kinematic chain i and the manipulator's end-effector. The shape of the end-effector is considered to be an equilateral triangle with altitude h. The geometric center of this triangle is defined as the end-effector's coordinates (x_e, y_e), while its angular position as the end-effector's coordinate α. The revolute joints are denoted by the points B_i (active), C_i (passive), and D_i (passive). The joint coordinates of these revolute joints are given by the angles θ_i, β_i, and α, respectively. The point A_i and the angle γ_i defines the localization of the prismatic joint. The joint coordinate of the prismatic joint is given by the position δ_i. The lengths of the links, $\|B_iC_i\| = l_1$ and $\|C_iD_i\| = l_2$, impose the kinematic constraints that are exploited to derive the inverse kinematic model hereafter.

With respect to the coordinate system O-xy, the position vector $\mathbf{r}_{D_i}$ can be written as

$$\mathbf{r}_{D_i} = \mathbf{r}_{C_i} + l_2 \begin{bmatrix} \cos \beta_i \\ \sin \beta_i \end{bmatrix} = \begin{bmatrix} x_e \\ y_e \end{bmatrix} + h \begin{bmatrix} \cos(\alpha + \lambda_i) \\ \sin(\alpha + \lambda_i) \end{bmatrix}, \tag{1}$$

while the position vector $\mathbf{r}_{C_i}$ as

$$\mathbf{r}_{C_i} = \mathbf{r}_{B_i} + l_1 \begin{bmatrix} \cos \theta_i \\ \sin \theta_i \end{bmatrix}, \tag{2}$$

and the position vector $\mathbf{r}_{B_i}$ as

$$\mathbf{r}_{B_i} = a_i \begin{bmatrix} \cos \lambda_i \\ \sin \lambda_i \end{bmatrix} + \delta_i \begin{bmatrix} \cos \gamma_i \\ \sin \gamma_i \end{bmatrix}, \tag{3}$$

where a_i the distance between the Coordinate System O-xy and the point A_i.

The substitution of Eqs. (2) and (3) in Eq. (1) yields the following kinematic constraint:

$$\begin{bmatrix} x_e \\ y_e \end{bmatrix} + h \begin{bmatrix} \cos(\alpha + \lambda_i) \\ \sin(\alpha + \lambda_i) \end{bmatrix} - a_i \begin{bmatrix} \cos \lambda_i \\ \sin \lambda_i \end{bmatrix} - \delta_i \begin{bmatrix} \cos \gamma_i \\ \sin \gamma_i \end{bmatrix} - l_1 \begin{bmatrix} \cos \theta_i \\ \sin \theta_i \end{bmatrix} = l_2 \begin{bmatrix} \cos \beta_i \\ \sin \beta_i \end{bmatrix}. \tag{4}$$

Equation (4) can be rewritten using the definition of the vector norm and some simplifications as:

$$\left\| \begin{bmatrix} \mu_i \\ \rho_i \end{bmatrix} - l_1 \begin{bmatrix} \cos \theta_i \\ \sin \theta_i \end{bmatrix} \right\| = l_2, \tag{5}$$

where

$$\begin{bmatrix} \mu_i \\ \rho_i \end{bmatrix} = \begin{bmatrix} x_e \\ y_e \end{bmatrix} + h \begin{bmatrix} \cos(\alpha + \lambda_i) \\ \sin(\alpha + \lambda_i) \end{bmatrix} - a_i \begin{bmatrix} \cos \lambda_i \\ \sin \lambda_i \end{bmatrix} - \delta_i \begin{bmatrix} \cos \gamma_i \\ \sin \gamma_i \end{bmatrix}. \tag{6}$$

The relation defined by Eq. (5) can be simplified as

$$-2l_1 \rho_i \sin \theta_i - 2l_1 \mu_i \cos \theta_i + \mu^2 + \rho_i^2 + l_1^2 - l_2^2 = 0. \tag{7}$$

Using this relation, the joint coordinates of the active revolute joints, given by the angles θ_i, can be calculated as follows:

$$\theta_i = 2 \tan^{-1} \frac{-E_{1i} \pm \sqrt{E_{1i}^2 + E_{2i}^2 - E_{3i}^2}}{E_{3i} - E_{2i}}, \tag{8}$$

where $E_{1i} = -2l_1 \rho_i$ $E_{2i} = -2l_1 \mu_i$ and $E_{3i} = \mu^2 + \rho^2 + l_1^2 - l_2^2$. The signal choice in this equation defines the working mode of the manipulator. This choice yields to eight possible working modes. In this manuscript, the plus sign in Eq. (8) is the choice for all the kinematic chains of the manipulator, as illustrated in Fig. 3.

Once the angles θ_i are known, the passive joint angles β_i can be calculated as follows:

$$\beta_i = \tan^{-1} \frac{\rho - l_1 \sin \theta_i}{\mu - l_1 \cos \theta_i}. \tag{9}$$

3. Redundancy Resolution Scheme

The aforementioned inverse kinematic modelling approach yields a set of three kinematic equations (one for each kinematic chain). The inverse kinematic problem presents an unique solution for the non-redundant 3$\underline{R}$RR manipulator. In other words, for a given end-effector's pose $\mathbf{X} = [x_e \ \ y_e \ \ \alpha]$, the active joint coordinates, $\boldsymbol{\Theta} = [\theta_1 \ \ \theta_2 \ \ \theta_3 \ \ \delta_1 \ \ \delta_2 \ \ \delta_3]$, are completely defined since $\delta_1 = 0$, $\delta_2 = 0$ and $\delta_3 = 0$. This is not true for the redundant manipulators. In these cases, for a given end-effector's pose $\mathbf{X}$, infinite solutions for the inverse kinematic problem can be found. The selection of a single solution among them is refereed as redundancy resolution that can be solved locally or globally.

The global approaches for redundancy resolution scheme seek to determine the optimal inputs for the redundant actuators for a given trajectory (tracking trajectory). In the literature, two main approaches for treating this problem can be found: the pre-positioning and the ongoing positioning approaches.[4,12] For the pre-positioning approaches, the optimal values of the redundant actuators' joint coordinates are kept constant during the task execution. Whilst, for the ongoing positioning approaches, the optimal values of the redundant actuators' coordinates may vary during the task execution. It has been shown that the latter approaches may yield improved dynamic performance,[12]

Table I. Notation of input values of the PKMs under investigation.

Manipulator	M	Θ_k					
R1	0	$[\theta_{1,k}$	$\theta_{2,k}$	$\theta_{3,k}$	0	0	$0]$
R2	1	$[\theta_{1,k}$	$\theta_{2,k}$	$\theta_{3,k}$	$\overline{\delta_1}$	0	$0]$
R3	1	$[\theta_{1,k}$	$\theta_{2,k}$	$\theta_{3,k}$	0	$\overline{\delta_2}$	$0]$
R4	1	$[\theta_{1,k}$	$\theta_{2,k}$	$\theta_{3,k}$	0	0	$\overline{\delta_3}]$
R5	2	$[\theta_{1,k}$	$\theta_{2,k}$	$\theta_{3,k}$	$\overline{\delta_1}$	$\overline{\delta_2}$	$0]$
R6	2	$[\theta_{1,k}$	$\theta_{2,k}$	$\theta_{3,k}$	$\overline{\delta_1}$	0	$\overline{\delta_3}]$
R7	2	$[\theta_{1,k}$	$\theta_{2,k}$	$\theta_{3,k}$	0	$\overline{\delta_2}$	$\overline{\delta_3}]$
R8	3	$[\theta_{1,k}$	$\theta_{2,k}$	$\theta_{3,k}$	$\overline{\delta_1}$	$\overline{\delta_2}$	$\overline{\delta_3}]$

but its complexity increases largely. Due to this important drawback, a pre-positioning approach is adopted hereafter. Due to the selection of this approach, the input values of the active prismatic joints (the redundant actuators) are the same during the task execution. Table I shows the input values, Θ_k, at the time step k for each PKM under investigation. The total number of time steps are denoted as K, yielding $k = 1, \ldots, K$. The line over the symbols denotes that these input values are constant during the task execution. This should be guaranteed by the optimization problem.

In this manuscript, a redundancy resolution scheme based on MPC technique is proposed and solved globally. In general terms, the MPC technique is an iterative method that solves individual optimization problems. These individual problems consider N future samples during the optimization process. The value N is called Prediction Horizon. This process is repeated for every time step moving the N future samples forward. Each individual optimization problem is going to be solved at every time step, k, yielding K optimization problems that can be formulated as

$$
\begin{aligned}
\underset{\vartheta \in \mathbb{R}^{3N+3}}{\text{minimize}} \quad & \frac{1}{2}\vartheta^T \mathbf{H}\vartheta \\
\text{subject to} \quad & \mathbf{A}_{eq} \cdot \vartheta = \mathbf{b}_{eq}, \\
& \mathbf{l}_b \leq \vartheta \leq \mathbf{u}_b,
\end{aligned}
\tag{10}
$$

where the cost function is described by a quadratic function while the constraints by linear relations. Due to these characteristics, these optimization problems can be classified as convex optimization problems.

Considering the redundancy resolution scheme using MPC technique proposed in Eq. (10), the decision variables, ϑ, for each optimization problem are related to $3N$ input values for each revolute active joint at every step time and three input values for each prismatic active joint (redundant actuators). In this way, the vector of the decision variables, $\vartheta \in \mathbb{R}^{3N+3}$, can be described by

$$
\vartheta = [\underbrace{\theta_{1,1} \quad \theta_{2,1} \quad \theta_{3,1}}_{j=1} \quad \cdots \quad \underbrace{\theta_{1,N} \quad \theta_{2,N} \quad \theta_{3,N}}_{j=N} \quad \overline{\delta_1} \quad \overline{\delta_2} \quad \overline{\delta_3}]^T,
\tag{11}
$$

where j refers to the sample time under evaluation. These decision variables are bounded by the physical limitations of the prototype's actuators. Their lower and upper bounds are described by the vectors $\mathbf{l}_b$ and $\mathbf{u}_b$, respectively. Moreover, these limitations are set to zero if the actuator is not active. For instance, $0 \leq \overline{\delta_1} \leq 0$ for the redundant R7 manipulator. The outcome of this optimization, the inputs of the active joints, can be used in the experimental prototype in a straightforward manner as described in the next section.

In each optimization problem, the equality constraint equations should guarantee the relation between the reference (desired trajectory) and the active joints inputs Θ via the inverse kinematic model for each time step k. These models are composed of nonlinear relations as denoted in Eq. (8). In order to include these nonlinear relations in the optimization problem, $(\mathbf{A}_{eq} \cdot \vartheta = \mathbf{b}_{eq})$, they should be linearized. This linearization is done by taking the first-order term of its Taylor expansion around the time instant defined by the considered sample. The partial derivatives of the trigonometric relations

have been approximated by the method of central differences. In this way, the equality constraints defined by the matrix $\mathbf{A}_{eq} \in \mathbb{R}^{(3N+3)\times(3N+3)}$ and the vector $\mathbf{b}_{eq} \in \mathbb{R}^{3N+3}$ guarantee the tracking of the reference trajectory at the N future samples.

Finally, the cost functions for the redundant PKMs should be defined. Due to the nature of the cost function, a quadratic function has been selected:

$$f(\boldsymbol{\vartheta}) = \frac{1}{2}\boldsymbol{\vartheta}^T \mathbf{H}\boldsymbol{\vartheta} = \frac{1}{2}\sum_{j=1}^{N}\left[\sum_{i=1}^{3}(\theta_{i,k-1} - \theta_{i,k})^2 + \sum_{i=1}^{3}(\overline{\delta}_i)^2\right]. \tag{12}$$

In fact, this cost function is composed of two terms. The first term, $\sum_{i=1}^{3}(\theta_{i,k-1} - \theta_{i,k})^2$, penalizes the motion of the active revolute joints. The second term, $\sum_{i=1}^{3}(\overline{\delta}_i)^2$, penalizes the motion of the active prismatic joints (redundant actuators). For both terms, the sub-index i indicates the kinematic chain and the sub-index j the sample time to be considered in the MPC problem. These choices penalize energy consumption by imposing minimal motion for performing the required task. Since the cost functions should be written in a matrix form (see Eq. (10)), the matrix $\mathbf{H}$ must be defined accordingly. Moreover, this matrix $\mathbf{H}$ should be positive semidefinite. For sake of illustration, $\mathbf{H}_{N=3} \in \mathbb{R}^{12\times12}$ can be described by

$$\mathbf{H}_{N=3} = \begin{pmatrix} 1 & 0 & 0 & -1 & 0 & 0 & 0 & 0 & 0 & 0 & 0 & 0 \\ 0 & 1 & 0 & 0 & -1 & 0 & 0 & 0 & 0 & 0 & 0 & 0 \\ 0 & 0 & 1 & 0 & 0 & -1 & 0 & 0 & 0 & 0 & 0 & 0 \\ -1 & 0 & 0 & 2 & 0 & 0 & -1 & 0 & 0 & 0 & 0 & 0 \\ 0 & -1 & 0 & 0 & 2 & 0 & 0 & -1 & 0 & 0 & 0 & 0 \\ 0 & 0 & -1 & 0 & 0 & 2 & 0 & 0 & -1 & 0 & 0 & 0 \\ 0 & 0 & 0 & -1 & 0 & 0 & 1 & 0 & 0 & 0 & 0 & 0 \\ 0 & 0 & 0 & 0 & -1 & 0 & 0 & 1 & 0 & 0 & 0 & 0 \\ 0 & 0 & 0 & 0 & 0 & -1 & 0 & 0 & 1 & 0 & 0 & 0 \\ 0 & 0 & 0 & 0 & 0 & 0 & 0 & 0 & 0 & 1 & 0 & 0 \\ 0 & 0 & 0 & 0 & 0 & 0 & 0 & 0 & 0 & 0 & 1 & 0 \\ 0 & 0 & 0 & 0 & 0 & 0 & 0 & 0 & 0 & 0 & 0 & 1 \end{pmatrix}, \tag{13}$$

according to the cost function described by Eq. (12).

For each time step, $k = 1 \ldots K$, the optimization problem described by Eq. (10) is solved and the optimal values for the decision variables are found, $\boldsymbol{\vartheta}^*$. The input values for the active joints are found as the optimal values of the decision variables for the actual time step under evaluation. In this way, the input values for the active joints at the time step k can be defined by $\theta_{1,k} = \boldsymbol{\vartheta}^*(1)$, $\theta_{2,k} = \boldsymbol{\vartheta}^*(2)$, $\theta_{3,k} = \boldsymbol{\vartheta}^*(3)$, $\overline{\delta}_1 = \boldsymbol{\vartheta}^*(3N+1)$, $\overline{\delta}_2 = \boldsymbol{\vartheta}^*(3N+2)$, and $\overline{\delta}_3 = \boldsymbol{\vartheta}^*(3N+3)$.

These convex optimization problems can be solved using the Interior Point Method.[27] This redundancy resolution scheme is exploited for planning the motion of the R2–R8 redundant manipulators for executing two trajectories described in the following section.

4. Description of the Experimental Campaign
In this section, the prototype is described. This versatile prototype can be exploited for comparing the energy consumption of the non-redundant (R1) and the redundant (R2-R8) PKMs during the execution of predefined tasks. Two tasks are investigated in this work. The trajectory planning of these tasks and the methodology for evaluating the energy consumption of the PKMs under study are also presented in this section.

4.1. Prototype's description
The prototype, depicted in Fig. 2, is actuated by six servomotors as illustrated by M1–M6 in Fig. 5. These servomotors are composed of brushless Maxon EC60 flat motors, Maxon planetary gearhead GP52C with a reduction rate of 3.5:1 and individual control boards Maxon EPOS2 50/5. In Fig. 5, the motors are illustrated by M1–M6, the control boards by C1–C6, and the power suppliers by PS1–PS2.

Table II. Prototype's geometrical parameters.

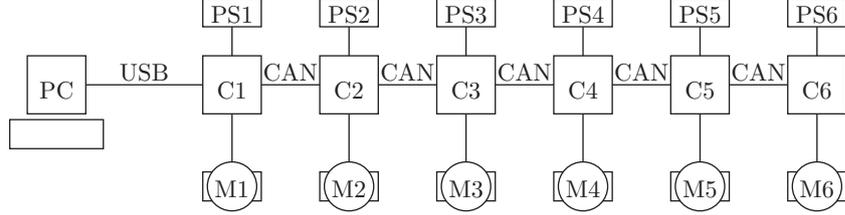|	$h(m)$	$a_i(m)$	$\gamma_i(deg)$	$\lambda_i(deg)$	$l_1(m)$	$l_2(m)$
$i=1$	59.7e-3	$259.8e-3$	180	90	0.191	0.232
$i=2$	59.7e-3	$259.8e-3$	60	−30	0.191	0.232
$i=3$	59.7e-3	$259.8e-3$	300	210	0.191	0.232

Fig. 5. Communication scheme between the boards and the computer.

The nominal torque of these motors is 0.257 N.m @ 3580 rpm. Due to the reduction rate of the planetary gearhead, the resulting available nominal torque of each set is 0.82 N.m @ 1200 rpm. The nominal current and maximum voltage of the control boards are 5A and 50 VDC, respectively. The motors M4–M6 drive the active prismatic joints. This linear motion is performed by a table system with ball screw HIWIN KK60-10-C-E-600-A-1-F0-S3. The stroke range of this system is 600 mm and its pitch is 10 mm.

The communication between the control boards is based on CAN Protocol. While the communication of the control board C1 (master) and the computer, illustrated by PC in Fig. 5, is via USB interface. A human–machine interface has been built in Matlab. In this environment, the users can define the control strategies to be employed by the control boards. There are several control strategies available in these boards (denoted as Modes). The experimental campaign described hereafter exploited the *Interpolated Position Mode*. In this mode, the user provides the desired positions and velocities at diverse time steps. This data is interpolated using splines by the board and is used as a reference signal to the control strategies. Moreover, in this mode, linear position feedforward, and position feedback control strategies are used to guarantee performance and robustness. The control parameters, the feedforward and feedback gains, have been adjusted manually.

Finally, Table II shows the values of the physical parameters of the prototype depicted in Fig. 2. Due to the manipulator's geometry, the active revolute joints are bounded to the interval $[-\pi, \pi]$ and the active prismatic joints to the interval $[-0.2, 0.2]$ (see Eq. (10)).

4.2. Trajectory planning

In an attempt to assess the impact of kinematic redundancy on the energy consumption of planar PKMs, the energy consumption of the non-redundant and the redundant PKMs (R1–R8) shown in Fig. 3 are compared. The energy consumption of these manipulators is evaluated during the execution of two different tasks denoted as I and II in Fig. 6. The profile of both trajectories are defined by a fifth degree polynomial function:

$$q(t) = a_0 + a_1 t + a_2 t^2 + a_3 t^3 + a_4 t^4 + a_5 t^5, \tag{14}$$

where t is time in seconds (s) and the coefficients $a_0 - a_5$ can be easily calculated by numerical integration if the initial and final values of position, velocity, acceleration, and time are provided. The use of a fifth-order polynomial function ensures that the trajectory of the end-effector is sufficiently smooth to avoid large transients at the start and end of the tasks' execution.

The trajectory I is a point-to-point task described by a horizontal straight line. The initial and final end-effector's poses for this task are $\mathbf{X}_0 = [0.1, -0.05, 0]$ and $\mathbf{X}_f = [0.1, 0.05, 0]$, respectively. The translational quantities are given in meters (m) and the rotational quantity is given in radians (rad). The initial and final values of the end-effector's velocity and acceleration are null. Using these conditions and the profile's definition (Eq. (14)), the coordinates of the end-effector, $(x_{eI}, y_{eI}, \alpha_I)$, are
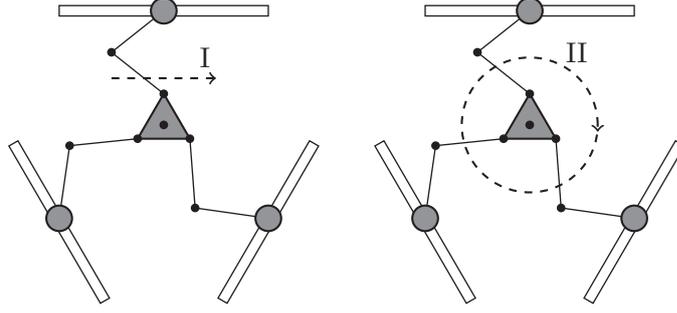
Fig. 6. Tasks I and II.

described as follows:

$$x_{eI}(t) = -1 + 0t + 0t^2 + 0.25t^3 - 0.1875t^4 + 0.0375t^5, \tag{15.1}$$

$$y_{eI}(t) = -0.05, \tag{15.2}$$

$$\alpha_I(t) = 0. \tag{15.3}$$

The trajectory II is a circle centered in the point $(0, 0)$ and the radius $0.1\ m$. The initial and final end-effector's pose for trajectory II are the same $\mathbf{X}_0 = \mathbf{X}_f = [0.1, 0, 0]$. Once again, the initial and final values of velocity and acceleration are null. Using the same approach exploited for the planning of trajectory I for the determination of trajectory II, the coordinates of the end-effector, $(x_{eII}, y_{eII}, \alpha_{II})$, can be described as follows:

$$x_{eII} = 0.1 \cdot \cos(q_{II}(t)), \tag{16.1}$$

$$y_{eII} = 0.1 \cdot \sin(q_{II}(t)), \tag{16.2}$$

$$\alpha_{II}(t) = 0, \tag{16.3}$$

where

$$q_{II}(t) = 0 + 0t + 0t^2 + 7.854t^3 - 5.8905t^4 + 1.1781t^5. \tag{17}$$

The task execution time is requested to be $T = 2s$ for both trajectories. The sampling time is considered to be $st = 0.004s$ yielding $K = 500$ time steps. In this way, $k = 1, \ldots, K$, $t(1) = 0$ and $t(K) = T = 2$. Due to this, 500 optimization problems, as described by Eq. (10), have to be solved. Each optimization problem is going to use $N = 10$ samples as prediction horizon.

4.3. Energy consumption evaluation

The redundancy resolution scheme provides the active actuators' inputs, $\mathbf{\Theta}_k$, for each time step, k. By taking into account the reduction rate of the gearhead and the pitch of the linear guide, these inputs can be used as reference signals to the actual prototype, $\mathbf{\Phi}_k = [\phi_{1,k} \quad \phi_{2,k} \quad \phi_{3,k} \quad \phi_{4,k} \quad \phi_{5,k} \quad \phi_{6,k}]^T$. These references signals can be used by the control strategies implemented at the control boards (C1–C6 in Fig. 2). Regarding the active revolute joints, the relation between these actuators' inputs and the references signals differs from the reduction rate, $\phi_{i,k} = 3.5\theta_{i,k}$, where $i = 1 \ldots 3$ and $k = 1 \ldots 500$. Regarding the active prismatic joints, the relation between these actuators' inputs and the reference signals differs from the reduction rate and the pitch, $\phi_{(i+3)} = 7\pi\bar{\delta}_i/0.01$ for $\bar{\delta}_i \neq 0$ otherwise $\phi_{(i+3)} = 0$, where $i = 1 \ldots 3$ and $k = 1 \ldots 500$.

Diverse discrete variables, such as actuators' currents, can be acquired during a task execution. Among them, the actuators' individual currents, $\mathbf{I}_k = [I_{1,k} \ldots I_{6,k}]^T$, and the actual actuators' angular positions, $\underline{\mathbf{\Phi}}_k = [\underline{\phi}_{1,k} \ldots \underline{\phi}_{6,k}]^T$, have been acquired, where $k = 1 \ldots 500$. The required voltage, $V_{i,k}$,
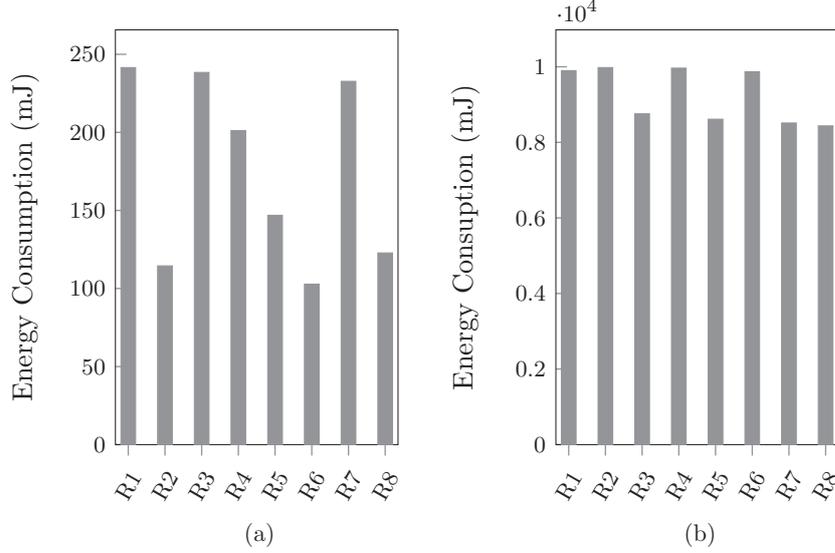
Fig. 7. Total power consumption for the eight configurations regarding the execution of (a) trajectory I and (b) trajectory II.

for driving each actuator at the time step k can be calculated by

$$V_{i,k} = K_b \cdot \frac{\phi_{i,k} - \phi_{i,k-1}}{t(k) - t(k-1)} + L \cdot \frac{I_{i,k} - I_{i,k-1}}{t(k) - t(k-1)} + R \cdot I_{i,k}, \tag{18}$$

where $K_b = 114$ mNm/A is the actuator's torque constant, $L = 0.864$ mH is the terminal inductance and $R = 1.1\Omega$ is the terminal resistance. The time derivatives have been approximated due to the discrete nature of the variables.

The energy consumption of each manipulator during the execution of any task, E_{total} can be calculated by taking the time integral of the electric power. Due to the discrete nature of the variables, the definite integral has been approximated using the trapezoidal rule:

$$E_{total} = \sum_{i=1}^{3+M} \left[\frac{st}{2} \sum_{k=1}^{K} (V_{i,k+1} I_{i,k+1} + V_{i,k} I_{i,k}) \right], \tag{19}$$

where $K = 500$ and M is described in Table I. Since SI units are used, the actuators' individual currents and required voltage are given in ampere (A) and volts (V), respectively. In this way, the E_{total} is given in joule (J).

5. Results
A comparison between the total energy consumption of the non-redundant and redundant R1–R8 manipulators, illustrated in Fig. 3, is done considering the execution of the trajectories I and II, illustrated in Fig. 6. These trajectories have been calculated according to the methodology described in Section 4.2. The execution of such trajectories by the redundant manipulators requires the use of a proper redundancy resolution scheme. In this work, the redundancy resolution scheme based on MPC proposed in Section 3 is exploited. Figure 7 compares the total average consumed energy: (a) during the experimental execution of trajectory I and (b) during the experimental execution of trajectory II. Both trajectories have been experimentally performed five times for the average calculation. The data are collected and the calculation of the total energy consumption (Eq. (19)) is carried out in an offline mode.

In general, one can conclude that the amount of electrical power required by the actuators of the redundant manipulators (R2–R8) have been less than or equal to the amount of electrical power
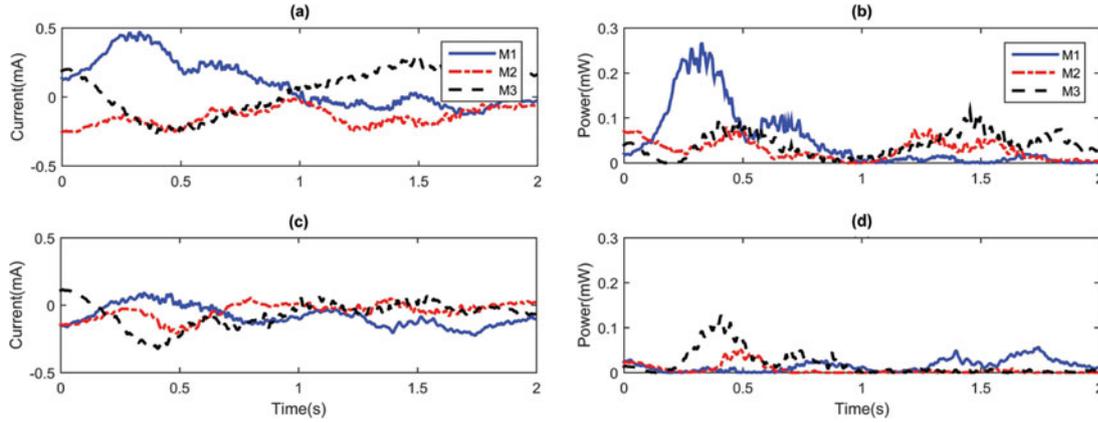
Fig. 8. Comparison between the experimental data during the execution of trajectory I: (a) Actuators' currents of the R1. (b) Actuators' electrical power of the R1. (c) Actuators' currents of the R8. (d) Actuators' electrical power of the R8.

required by the actuators of the non-redundant manipulator (R1). This conclusion can be drawn for both trajectories. This indicates that the inclusion of the kinematic redundancies have been positive regarding the consumption of electrical energy. In fact, the active prismatic joints of the redundant manipulators can be moved to a proper configuration (reconfiguration capability). In this proper configuration, the singularities are avoided during the motion yielding an important reduction of the energy consumption. This fact demonstrates the potential of the kinematically redundant manipulators regarding energy efficiency.

Regarding the energy consumption for the execution of the trajectory I, it can be concluded that the redundant manipulators R2 (1 kinematic redundancy) and R6 (2 kinematic redundancies) have considerably consumed smaller amounts of energy than the others. The fact that the redundant manipulator R8 have consumed a greater amount of electrical power than the both R2 and R6 may be puzzling since previous numerical studies regarding the same PKMs have shown that redundant manipulators have always been capable to enforce a reduction on power consumption.[26] The authors believe that the main reason for this discrepancy is the fact that there is no way to guarantee that the actuators and their assembles are in fact the same for all kinematic chains.

Regarding the energy consumption for the execution of the trajectory II, it can be concluded that only the redundant manipulators R3 (1 kinematic redundancy), R5/R7 (2 kinematic redundancies), and R8 (3 kinematic redundancies) have consumed smaller amounts of electrical power than the non-redundant one. Since the manipulator is not symmetric (due to the links' configurations), the power consumption of the manipulators R2, R3, and R4 (1 kinematic redundancy) for the execution of the trajectory II (symmetric trajectory regarding the positions of linear guides) should not be the same. This can be verified experimentally by observing that R3 have consumed a smaller amount of electrical power than the manipulators R2 and R4. The same conclusions can be drawn regarding the consumption of the manipulators R5, R6, and R7 (two kinematic redundancies). In fact, the redundant actuator δ_2 is the main responsible for the reduction of electrical consumption. This conclusion can be drawn since this redundant actuator is active at the manipulators R3, R5, R7, and R8.

For sake of completeness, the actuator's currents and power consumption are depicted in Figs. 8 and 9 for the manipulators R1 and R8. Regarding the execution of the trajectory I (Fig. 8), one can verify that the currents and the electrical power of the redundant manipulator have been considerably lower than the data related to the non-redundant manipulator. The same cannot be verified during the execution of trajectory II (Fig. 9). These results are in line with the data shown in Fig. 7, where the reduction on the power consumption was about 50% for the trajectory I and 10% for the trajectory II considering three levels of kinematic redundancy. In this way, one can conclude that the amount of reduction on power consumption is dependent not only on the exploited kinematic redundancy (as previously discussed), but also on the task to be executed.
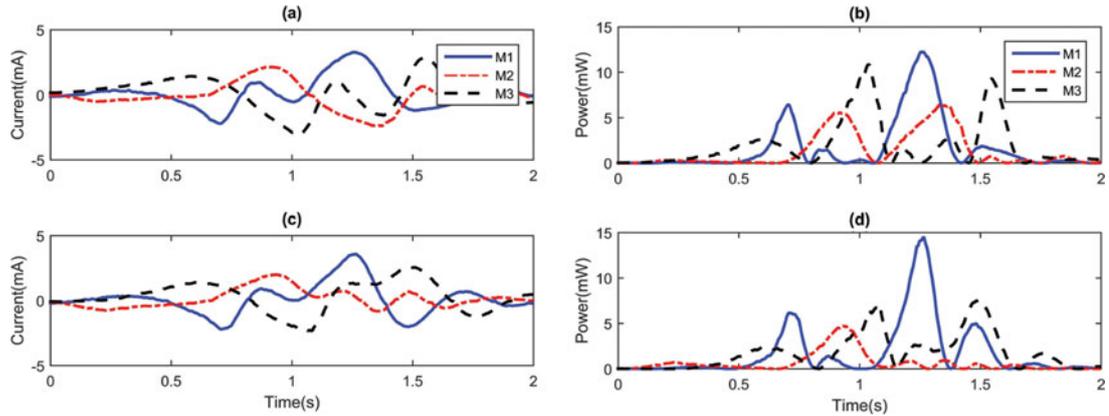
Fig. 9. Comparison between the experimental data during the execution of trajectory II: (a) Actuators' currents of the R1. (b) Actuators' electrical power of the R1. (c) Actuators' currents of the R8. (d) Actuators' electrical power of the R8.

6. Conclusions

In this manuscript, the impact of kinematic redundancies in the energy consumption of a planar PKM is experimentally assessed. The experimental campaign has been carried out using the redundant 3P̲RRR redundant. Up to three levels of kinematic redundancies can be evaluated using this prototype by locking or actuating the prismatic joints yielding eight possible configurations. Because of the presence of the kinematic redundancies, the inverse kinematic problem presents infinity solutions. The selection of a solution among the possibilities was performed by a redundancy resolution scheme based on the MPC technique. The average of the energy consumption of the eight configurations have been experimentally measured.

It can be concluded that the energy consumption of the non-redundant parallel manipulator 3R̲RR can be reduced by the inclusion of a proper kinematic redundancy scheme. This conclusion confirms previous results based on numerical investigations. Nevertheless, the possible energy consumption reduction is highly dependent on the task to be executed and on how the kinematic redundancies are exploited.

In general, the potential of kinematically redundant manipulators regarding energy efficiency should be carefully investigated. For instance, an important limitation in this study was the use of the pre-positioning strategy for the redundant actuators. The use of different strategies could yield improved results.

References

1. M. M. da Silva, L. P. R. de Oliveira, O. Bruls, M. Michelin, C. Baradat, O. Tempier, J. De Caigny, J. Swevers, W. Desmet, and H. Van Brussel, "Integrating structural and input design of a 2-DOF high-speed parallel manipulator: A flexible model-based approach," *Mech. Mach. Theory* **45**(11), 1509–1519 (2010). https://doi.org/10.1016/j.mechmachtheory.2016.05.004

2. Y. Li and G. M. Bone, "Are Parallel Manipulators More Energy Efficient?," *Proceedings of the IEEE International Symposium on Computational Intelligence in Robotics and Automation* (2001) pp. 41–46. https://doi.org/10.1109/CIRA.2001.1013170

3. G. Clement and A. Jorge, "Singularity analysis of closed-loop kinematic chains," *IEEE Trans. Robot. Autom.* **6**(3), 281–290 (1990). https://doi.org/10.1109/70.56660

4. J. Kotlarski, B. Heimann and T. Ortmaier, "Influence of kinematic redundancy on the singularity-free workspace of parallel kinematic machines," *Fron. Mech. Eng.* **7**(2), 120–134 (2012). https://doi.org/10.1007/s11465-012-0321-8.

5. M. G. Mohamed and C. M. Gosselin, "Design and analysis of kinematically redundant parallel manipulators with configurable platforms," *IEEE Trans. Robot.* **21**(3), 277–287 (2005). https://doi.org/10.1109/TRO.2004.837234

6. S. H. Cha, T. A. Lasky and S. A. Velinsky, "Singularity Avoidance for the 3-RRR Mechanism Using Kinematic Redundancy," *Proceedings of IEEE International Conference on Robotics and Automation (ICRA)* (2007) pp. 1195–1200. https://doi.org/10.1109/ROBOT.2007.363147.

7. T. D. Thanh, J. Kotlarski, B. Heimann and T. Ortmaier, "Dynamics identification of kinematically redundant parallel robots using the direct Search method," *Mech. Mach. Theory* **52**, 277–295 (2012). https://doi.org/10.1016/j.mechmachtheory.2012.02.002

8. C. Gosselin, T. Laliberte and A. Veillette, "Singularity-free kinematically redundant planar parallel mechanisms with unlimited rotational capability," *IEEE Trans. Robot.* **31**(2), 457–467 (2015). https://doi.org/10.1109/TRO.2015.2409433

9. J. Kotlarski, B. Heimann and T. Ortmaier, "Experimental Validation of the Influence of Kinematic Redundancy on the Pose Accuracy of Parallel Kinematic Machines," *Proceedings of IEEE International Conference on Robotics and Automation (ICRA)* (2011) pp. 1923–1929. https://doi.org/10.1109/ICRA.2011.5980056

10. F. Xie, X. J. Liu and J. Wang, "Performance evaluation of redundant parallel manipulators assimilating motion/force transmissibility," *Int. J. Adv. Robot. Syst.* **8**(5), 113–124 (2011). https://doi.org/10.5772/50904.

11. Y. Zhao and F. Gao, "Dynamic formulation and performance evaluation of the redundant parallel manipulator," *Robot. Comput.-Integr. Manuf.* **25**(4–5), 770–781 (2009). https://doi.org/10.1016/j.rcim.2008.10.001

12. J. V. Fontes and M. M. da Silva, "On the dynamic performance of parallel kinematic manipulators with actuation and kinematic redundancies," *Mech. Mach. Theory* **103** 148–166 (2016). https://doi.org/10.1016/j.mechmachtheory.2016.05.004

13. M. Luces, J. K. Mills and B. Benhabib, "A review of redundant parallel kinematic mechanisms," *Intell. Robot Syst.* **86**(2), 175–198 (2017). http://dx.doi:10.1007/s10846-016-0430-4

14. A. Muller, "On the terminology and geometric aspects of redundant parallel manipulators," *Robotica*, **31**(1), 137–147 (2013). http://doi:10.1017/S0263574712000173

15. J. M. Ahuactzin and K. K. Gupta, "The kinematic Roadmap: A motion planning based global approach for inverse kinematics of redundant robots," *IEEE Trans. Robot. Autom.* **15**(4), 653–669 (1999). https://doi.org/10.1109/70.781970

16. B. Siciliano, "Kinematic control of redundant robot manipulators: A tutorial," *J. Intell. Robot. Syst.* **3**, 201–212 (1990). https://doi.org/10.1007/BF00126069

17. J. C. Santos and M. M. da Silva, "Redundancy resolution of kinematically redundant parallel manipulators via differential dynamic programming," *J. Mech. Robot.* **9**(4), 041016 (2017) https://doi.org/10.1115/1.4036739

18. F. O. M. Joseph, L. Behera, T. Tamei, T. Shibata, A. Dutta, A. and A. Saxena, "On redundancy resolution of the human thumb, index and middle fingers in cooperative object translation," *Robotica* **35**(10), 1992–2017 (2017). http://dc.doi.org/10.1017/S0263574716000680

19. T. Faulwasser and R. Findeisen, "Nonlinear model predictive control for Constrained output path following," *IEEE Trans. Autom. Control* **61**(4), 1026–1039 (2016). https://doi.org/10.1109/TAC.2015.2466911

20. M. Bock and A. Kugi, "Real-time nonlinear model predictive path-following control of a laboratory tower crane," *IEEE Trans. Control Syst. Technol.* **22**(4), 1461–1473 (2014). https://doi.org/10.1109/TCST.2013.2280464

21. G. B. Avanzini, A. M. Zanchettin and P. Rocco, "Constrained model predictive control for mobile robotic manipulators," *Robotica* **36**(1), 1992–2017 (2018). http://dx.doi:10.1017/S0263574717000133

22. K. Belda, J. Bohm and M. Valasek, "State-space generalized predictive control for redundant parallel robots," *Mech. Based Des. Struct. Mach.* **31**(3), 413–432 (2003). https://doi.org/10.1081/SME-120022857

23. S. Wen, G. Qin, B. Zhang, H. K. Lam, Y. Zhao and H. Wang, "The study of model predictive control algorithm based on the force/position control scheme of the 5-DOF redundant actuation parallel robot," *Robot. Autom. Syst.* **79**, 12–25 (2016). https://doi.org/10.1016/j.robot.2016.02.002

24. T. Hufnagel, C. Reichert and D. Schramm, "Centralized non-linear model predictive control of a redundantly actuated parallel manipulator," *New Trends Mech. Mach. Sci.* **7**, 621–629 (2013). https://doi.org/10.1007/978-94-007-4902-3-6

25. G. Lee, S. Park, H. Kim, J. Jeong and J. Kim, "Energy saving effect mapping of redundant actuation in workspace," *Procedia CIRP* **26**, 145–149 (2015). https://doi.org/10.1016/j.procir.2014.07.071

26. A. G. Ruiz, J. V. C. Fontes and M. M. da Silva, "The Influence of Kinematic Redundancies in the Energy Efficiency of Planar Parallel Manipulators," *Proceedings of the ASME International Mechanical Engineering Congress and Exposition*, No. IMECE2015-50278, https://doi.org/10.1115/IMECE2015-50278

27. S. Boyd and L. Vandenberghe, *Convex Optimization* (Cambridge University Press, Cambridge, 2014).